JOURNAL OF AIRCRAFT
Vol. 34, No. 3, May–June 1997

Experimental and Numerical Investigation of Rotor Aerodynamics in Forward Flight

T. Berenger,* D. Favier,† C. Maresca,† and E. Berton‡
University of Aix-Marseille I & II, 13009 Marseille, France

This paper concerns an experimental and numerical investigation of the aerodynamic field of a model rotor in forward flight. The study emphasizes the characterization of the flowfield in the immediate vicinity of the blade and in its near wake. The analysis of the blade aerodynamics is supported by measurements performed on the overall airloads, the three-dimensional velocity field around the blade and in the wake (determined by means of laser Doppler anemometry measurements), and the geometry of the tip vortex path. The corresponding data results allow the correlation of typical velocity profiles to the vortex characteristics parameters. From the computational approach, the prediction efficiency of a prescribed wake analysis code and its improvement are checked by direct comparisons with experiments performed either on the tip vortex path, or on the three-dimensional velocity field and the circulation distribution along the blade span.

Nomenclature

A = rotor disc area, πR^2, m^2
b = number of blades
C_l, C_d = lift and drag coefficients
C_T = rotor thrust coefficient, $T/\rho A(\Omega R)^2$
C_Q = rotor power coefficient, $Q/\rho A(\Omega R)^3$
c = blade chord, 0.05 m
O_{xyz} = coordinates system, in Fig. 1
Q = rotor torque, Nm
R = rotor blade radius, 0.75 m
Ro = root cut out, 0.22R
R_v = vortex core radius, m
r = radial distance from the rotation axis, m
T = rotor thrust, N
u, l = upper and lower side of the blade sections
u, v, w = radial, tangential, and axial velocities
V_∞, V_e = freestream axial velocity and tip speed ($V_e = \Omega R$), m/s
α_s = rotor shaft angle, deg
Γ = blade circulation, m^2/s
θ_v = blade twist angle, deg
$\theta_{0.75}$ = collective pitch angle at r/R = 0.75, deg
μ = advance ratio, $V_\infty/\Omega R$
σ = rotor solidity, $bc/\pi R$
Ψ = blade azimuth, deg
Ω = angular rotational frequency, 143 rad/s

Presented as Paper 96-0676 at the AIAA 34th Aerospace Sciences Meeting, Reno, NV, Jan. 15–18, 1996; received Feb. 11, 1996; revision received Aug. 10, 1996; accepted for publication Nov. 12, 1996.

*Graduate Student, Institut de Recherche sur les Phénomènes hors Équilibre/Laboratoire Aerodynamique Subsonique Instationnaire, Unité Mixte de Recherche 138, Centre National de la Recherche Scientifique, 163, Avenue de Luminy, Case 918.

†Senior Research Scientist, Institut de Recherche sur les Phénomènes hors Équilibre/Laboratoire Aerodynamique Subsonique Instationnaire, Unité Mixte de Recherche 138, Centre National de la Recherche Scientifique, 163, Avenue de Luminy, Case 918. Member AIAA.

‡Research Scientist, Institut de Recherche sur les Phénomènes hors Équilibre/Laboratoire Aerodynamique Subsonique Instationnaire, Unité Mixte de Recherche 138, Centre National de la Recherche Scientifique, 163, Avenue de Luminy, Case 918. Member AIAA.

Introduction

THE accurate prediction of local and overall airloads of helicopter rotor in forward flight requires a realistic and detailed knowledge of the vortex trajectories trailed from the blade tips, as well as the corresponding velocity field induced both by the vortical wake and by the rotor blades. The accurate determination of such relevant flow parameters has been challenged by many aerodynamicists over the past 20 years. Sophisticated experimental methods, based particularly on laser Doppler anemometry (LDA) techniques, have been developed to determine local blade characteristics as circulation, velocity field,[1–5] and other data such as wake geometry and interactions.[6–8] Results are expected to describe accurately the complete wake geometry, and thus will constitute a valuable aid in the numerical modeling of the rotor aerodynamics.

The main objective of this paper, in extension of previous works,[9,10] concerns an experimental and numerical investigation of the local and overall rotor aerodynamics in forward flight. The experimental approach has been based on extensive measurements, including six-component rotating balance, hot wires, and long focal length velocimetry laser (LDA) techniques. The three-dimensional time-dependent flowfield around the blade and in its near wake have been investigated by means of LDA measurements of the three-dimensional velocity field, and also by measurements of the tip vortex trajectories that are trailed by the tips at different blade azimuthal positions. Such experimental data are then used to provide a detailed characterization of the flow in the immediate vicinity of the blade and to identify the local influence of the vortex filaments system on the blade section aerodynamics [blade vortex interaction (BVI)]. Additionally, the results obtained from the velocity profiles measurements in the near wake also provide typical parameters concerning the development of the tip vortices along their paths (e.g., the evolution of the vortex core size along its path, and the evolution of vortex intensity before and at BVI).

The numerical approach has been based on a prescribed wake analysis method (METAR code[11,12]). The prediction efficiency of such a method, which uses a lifting line for the blade modeling, has been checked by direct comparisons with different sets of data measurements, including the tip vortex path, the three-dimensional velocity field, and the circulation distribution measured along the blade span at a given blade rotational azimuth. Based on such comparison results, several improvements of this numerical method using a free-wake analysis have been obtained.

Experimental Setup and Measurements Methods

The experiments were conducted at the Aerodynamique Subsonique Instationnaire Laboratory on a scale model rotor installed in the V2 test section of the S1L subsonic wind tunnel (octagonal test section, 4 m; length, 8 m; and freestream velocity, 5 m/s $\leq V_\infty \leq$ 60 m/s). Figures 1a and 1b show the model rotor mounted for testing in the forward-flight configuration.

The model rotor consists of a fully articulated rotor hub, which can be equipped with interchangeable sets of blades. The different sets of rotor blades, designed so that the radii of the corresponding blade remain constant and equal to $R = 0.75$ m, correspond to various combinations of blade twist, airfoil section, and tip shape. The different tip geometries: swept, tapered, parabolic, and rectangular, provide the same rotor solidity ($\sigma = 0.08403$ for $b = 4$). The tests have been run at a constant angular velocity $\Omega = 143$ rad/s, i.e., a tip speed of about 110 m/s. Tip blade Reynolds number and Mach number were therefore removed from full scale, although the advance ratio was kept at a realistic value: $\mu = 0.20$. Consequently, the present work does not report on eventual tip vortex and BVI compressibility effects that can occur on full-scale rotors.

Several measurement techniques for surveying the flow in the near- and far-wake regions and around the blades have been developed,[13,14] including X-wire anemometry and LDA technique with long focal length (2–2.5 m). Figure 1b shows the fixed coordinates system (O_{xyz}) used for the velocity component u, v, w measurements and the wake survey in forward flight.

Overall forces (averaged thrust and torque) were performed by means of a six-component balance mounted on the rotor hub. Measurements were averaged over 300 rotations of the rotor. The full-scale values of forces and moments delivered by the balance in x and y directions are, respectively, 800 N and 150 Nm, and in the z direction 2000 N and 300 Nm, respectively. The global experimental error, including nonlinearity and hysteresis effect of the sensors, is about 2% and is close to 4% in the case of local stall on blades and strong BVI.

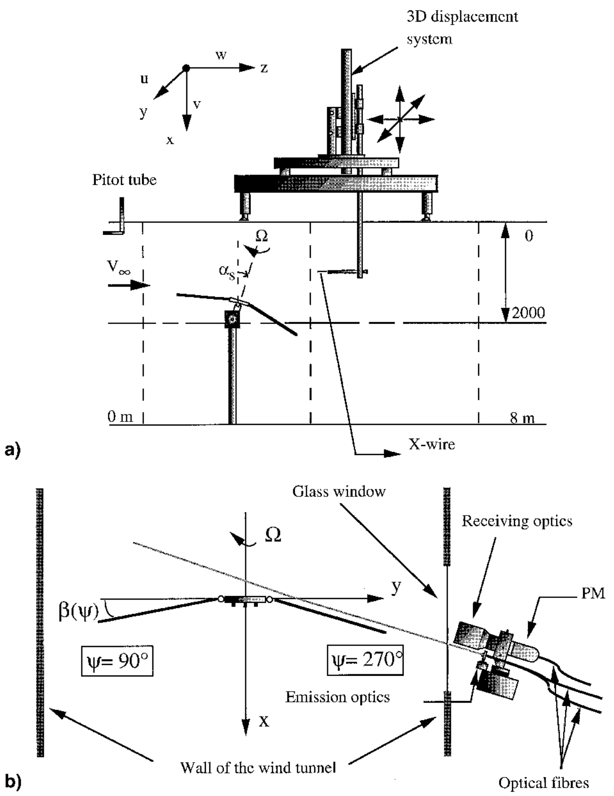

Fig. 1 Schematics of the a) X hot-wire anemometry system and b) the LDA system.

Tip vortex paths were measured by smoke visualization in the region very close to the blade and by means of a hot-wire technique, which allows the determination of the wake position as a function of the blade azimuth. Using these techniques, a tip vortex location can be determined with an accuracy of about 1 mm in r, and 0.2 mm in z, resulting in $\Delta r/R \leq 1/750$ and $\Delta z/R \leq 1/500$. In the cases of tip trajectories wandering, occurring during local stall or strong BVI, the uncertainty on $\Delta r/R$ can reach 0.05.

The three-dimensional velocity field was measured by two complementary techniques: 1) LDA operating in a backscatter mode close to the blade surface (along a close contour surrounding the blade section) and 2) an X-wire probe in the middle and far wake. The X-wire probe was positioned behind the rotating plane by means of an automated traversing mechanism (see Fig. 1a). Near the blade, the velocity components u, v, and the redundant axial component w were determined by LDA in the fixed coordinates system defined in Fig. 1b. The flow was seeded with a mixture of oil and water resulting in 1-μm-diam particles. The dimensions of the measuring volume were $0.2 \times 0.5 \times 0.3$ mm, with 84 fringes (interfringe = 2.7 μm). The initiation and synchronization of the data were realized by means of a photocell. Measurements were phase-averaged over 300 rotations of the rotor with an accuracy estimated[14] at 4% for the w component and 6% for u and v components, or, respectively, 8 and 9% in the case of instabilities caused by stall and BVI. The value of the corresponding azimuth is delivered by an encoder with a precision of ± 0.36 deg.

Rotor Model

The model used for the forward-flight configuration has been initially derived at Eurocopter France (METAR code) and is described in more detail in Refs. 11 and 12. The theoretical approach and the numerical resolution have been based on the following main elements: each blade is represented by a lifting line at the quarterchord of the airfoils, and the wake is constituted by the tip vortex filaments whose intensity Γ is varying both with the radial section and the blade azimuth.

The input data are the geometrical and operating rotor conditions (b, V_∞, θ, Ω, α_s, μ, ...), and the blade airfoil characteristics (C_l, C_d). The thrust coefficient first has to be estimated to generate the velocity field on the rotor disk and to define the associated geometry of the wake, although this thrust coefficient is recalculated during the numerical procedure. At this initial step, the induced velocities on the blade are modeled using a Meyer-Drees model,[15] which assumes that the bound circulation is constant along the blade span and varies sinusoidally with Ψ.

The initial wake is generated from the tip vortex contraction and convection laws as given in Refs. 7–14, and 16 for the forward-flight configuration. In the present model simplified formulations of the envelope and form functions (E, G) have been used[11,12] when compared to those given in Refs. 7–15. Once the initial wake geometry is determined, the influence coefficient matrix can be built.

Figures 2a and 2b show the discretization mesh used for the rotor disk and wake description. The rotor disk is divided into 11 radial stations ($0 \leq j \leq 10$) and 24 azimuthal positions ($0 \leq i \leq 23$), where $i = 0$ corresponds to $\Psi = 0$ deg, in Fig. 2a. Such a discretization results from an optimization procedure[12,14] providing a compromise between the time required for convergence on the velocity field and the accuracy of calculation results. The calculation points on the blades are noted $PR(i, j)$, whereas the wake points are denoted $PS(i, j, k)$, where k represents the vortex age in the wake and varies from $k = 0$ (at its emission on the blade) to $k = 72$, with an azimuth step of 15 deg (see Fig. 2b). At each azimuthal step, the vorticity

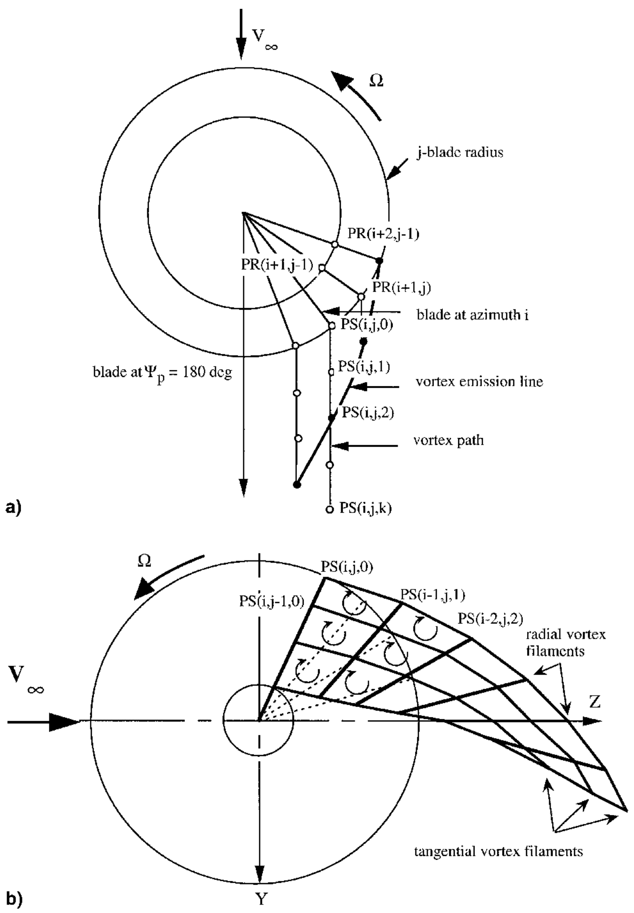

Fig. 2 a) Rotor disk mesh and b) wake mesh.

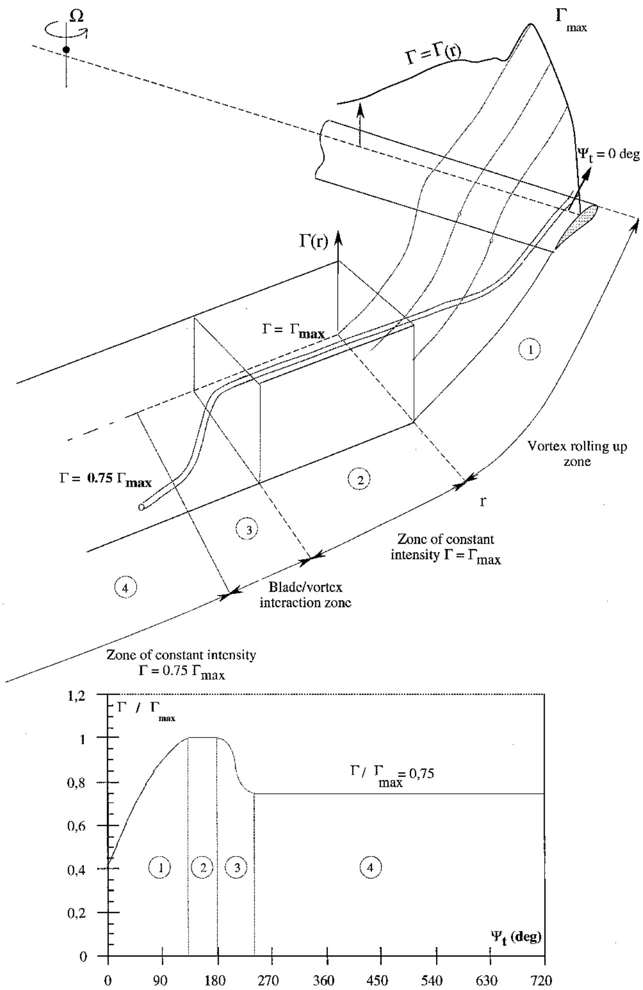

Fig. 3 Modeling of vortex intensity with age.

is shed in the wake and is conserved on a mesh element as it is convected downstream. The influence of all the elements induces the velocity changes at the calculation points on the rotor disk.

The previously defined prescribed wake calculation model has been improved using a free-wake analysis based on an initial wake geometry deduced from the present test data. Additionally, to this wake geometry distortion, the experimental evolution of the tip vortex core and its intensity along the path has been also included in the numerical procedure. The results of this free-wake analysis depend on R_v. Therefore, different tip vortex trajectories have been calculated for different R_v and then compared to experiments. It has been shown (Ref. 14) that the better agreement between calculation and experiment of a vortex trajectory trailed from the blade tip at azimuth Ψ_b was obtained when R_v satisfied the following equation:

$$R_v(\Psi_b, \Psi_t) = a(\Psi_t)\sin\Psi_b + b(\Psi_t)\cos\Psi_b + c(\Psi_t)$$

Where Ψ_t is the age of the vortex counted from the blade azimuthal position Ψ_b, and a, b, and c are functions tabulated in Ref. 14 for $\alpha_s = -6$ and -12 deg.

Moreover, the agreement between the calculated and experimental tip vortex path can be improved by modeling the variation in time of the vortex intensity along four phases:

1) The first one corresponds to the rolling up of the lattices trailed from the blade between the location of the maximum circulation and the tip. The tip vortex is then built up between $\Psi_t = 0$–105 deg (see Fig. 3), while its intensity varies from 40% of Γ_{max} to Γ_{max}.

2) The second concerns a zone of constant intensity (Γ_{max}) from $\Psi_t = 105$ to 180 deg that corresponds to the first interaction with the following blade.

3) The third gives the decrease of the intensity to 75% of Γ_{max} at $\Psi_t = 225$ deg through a third-degree polynomial.

4) Finally, during the fourth phase, the intensity keeps a constant value for more than one revolution, so that the calculation remains insensitive to intensity variation during this phase.

Moreover, the free-wake analysis option considered in the present calculation model consists of convecting the vortex filaments using the time-dependent-induced velocity field as locally calculated.[14] In such a way the improvement given to the model includes a free-wake analysis in which the geometry and intensity of the trailing vortices are consistent with the blade loading as determined by the induced velocity field.

From the previously defined rotor and wake representations, the next step of the procedure is to proceed through an iterative loop where the blade circulation, the induced velocities on blade, and the vortical wake are calculated, until convergence is reached on the velocity field. Then the final values of C_T, Γ, and the induced velocities on blade are obtained as outputs.

Comparisons Between Calculation and Experiment

In the present investigation, both overall and local aerodynamic characteristics of the flowfield through the rotor have been determined on different rotor configurations. The following experimental and numerical results are focused on the results corresponding to a rotor with rectangular blade tips and considered at the following operating parameters: $b = 2$, $\theta = 10$ deg, $\alpha_s = -6$ and -12 deg, and $\mu = 0.20$.

The experimental data obtained in this forward-flight configuration concern first the measurements of the three-dimensional velocity field in the rotor wake, the tangential velocity around the blade, and the circulation distribution along the span.

For the purpose of the circulation measurement around the blade at a given radial section r, the LDA method is applied along a close contour surrounding the blade section into consideration. As shown in Fig. 4, the method principle used[13,14] for general flight conditions consists of measuring, at a given blade azimuth (Ψ_b = 270 deg), the two-velocity components that are tangent to the closed rectangular contour surrounding the blade section. The circulation is then obtained by

$$\Gamma = \oint V \, \mathrm{d}l = \sum_{i=1}^{i=26} V_i \, \mathrm{d}M_i$$

The number of discretization points along the close contour have been selected at $N = 26$ to get a good accuracy in determining Γ from the previous formulation.

An example of the tangential velocity profiles obtained is shown in Fig. 5. As described previously, the tangential velocity field around the blade is determined as a function of the blade azimuth by means of velocimetry laser measurements performed at two fixed points (nos. 3 and 11 in Fig. 4), located on the lower and upper side of the blade section and at the radial section r/R = 0.95. On the upper side of the airfoil, the deficit of the tangential velocity localizes accurately the blade passage at Ψ = 90 and 270 deg. On the lower side, the velocity profile in Fig. 5 shows successively as a function of Ψ: a first peak (corresponding to the influence of the blade passage on the measurement point), and then, two consecutive peaks of velocity (with a gradient velocity inversion), which reflects the influence of the tip vortex shed by the preceding blade. The circulation Γ around the blade section at a given r/R corresponds therefore to the sum of the circulations calculated for each branch of the contour defined in Fig. 4. Different measurements of Γ obtained in the same operating rotor conditions, but when varying the dimensions of the box, have been performed.[13] It has been shown that Γ is sensitive to the contour of integration: Γ grows as long as the box dimensions are enlarged in a region very close to the blade section, then keeps a constant value when the rectangular dimensions of the box z/c and x/c are such that $1.2 \leq z/c \leq 2$ and $0.7 \leq x/c \leq 1$. It was inferred that the values z/c = 1.3 and x/c = 0.9, chosen in the present work, allowed a good accuracy for circulation measurement.

Figure 6 shows a comparison of calculation and experiment of the circulation distribution along the span at Ψ_b = 270 deg. The results show that the calculated distribution of circulation is in good agreement with the experimental data. Moreover, the calculation results reveal a specific behavior in the circulation distribution over the inner part of the blade span, and exhibits the presence of a peak close to r/R = 0.5. Such an increase on the calculated Γ distribution is because of the blade/vortex influence that results from the vortex filament trailed by the blade tip at Ψ_b = 90 deg. In Fig. 7, the comparison of calculation and experiment for $\alpha_s = -12$ deg and μ = 0.20 leads to similar trends. The circulation distribution obtained from the numerical model using the present free-wake analysis procedure is shown to correlate well with the experimental Γ distribution.

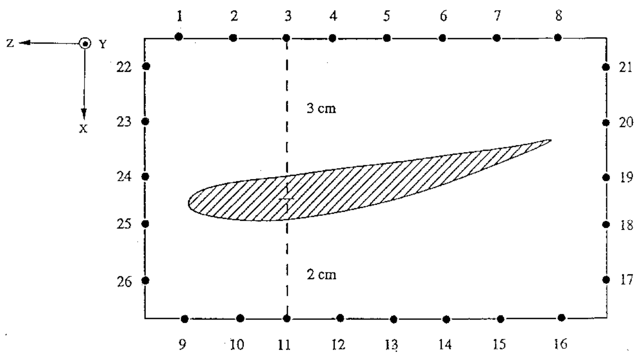

Fig. 4 Contour surrounding a given blade section in forward flight.

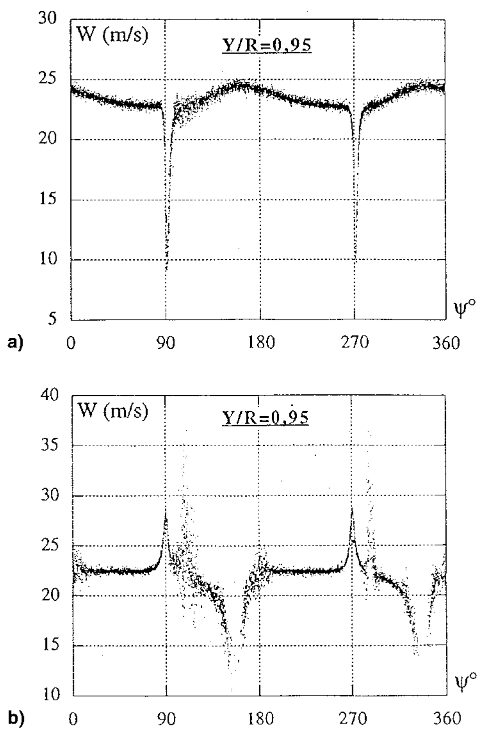

Fig. 5 Tangential velocity field around the blade: a) upper and b) lower sides. b = 2, $\alpha_s = -6$ deg, μ = 0.20, θ = 10 deg, and Ψ_b = 270 deg.

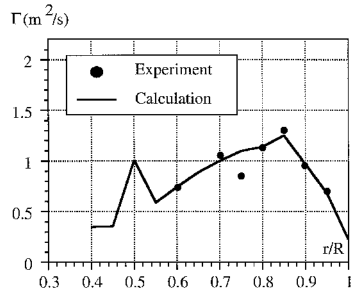

Fig. 6 Calculation/experiment comparison on circulation distribution along the blade span, $\alpha_s = -6$ deg, μ = 0.2, θ = 10 deg, and Ψ_b = 270 deg.

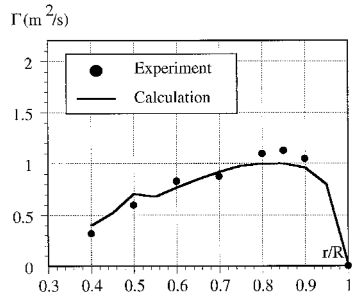

Fig. 7 Calculation/experiment comparison on circulation distribution along the blade span. $\alpha_s = -12$ deg, μ = 0.2, θ = 10 deg, and Ψ_b = 270 deg.

In Fig. 8, the results concerning the tip vortex lines in the longitudinal plane (y/R, z/R) measured at $\alpha_s = -12$ deg and $\mu = 0.20$ for $\Psi_b = 0$, 90, 180, and 270 deg, are compared with the cycloidal wake model. The cycloidal wake is based on the mean induced velocity (averaged in time) of the flowfield through the rotor disk. In each case, the cycloidal wake model is shown to be in a good agreement in the (y/R, z/R) plane with measurements, confirming previous works. For the vertical and lateral planes (x/R, y/R) and (x/R, z/R), this cycloidal model significantly deviates from experiments. It is clear that the calculation method has to include wake distortion[7–14] along the $x/R = x/R(\Psi)$ coordinate for predicting accurately local aerodynamics along the blade span.

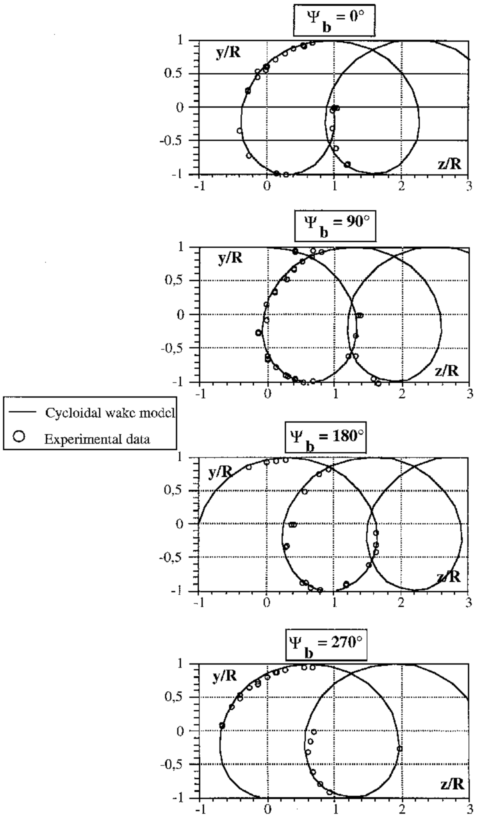

Fig. 8 Emission lines $y = y(z)$: experiments/cycloidal wake model. $b = 2$, $\alpha_s = -12$ deg, $\mu = 0.2$, $\theta = 10$ deg, and $V_\infty = 21.4$ ms^{-1}.

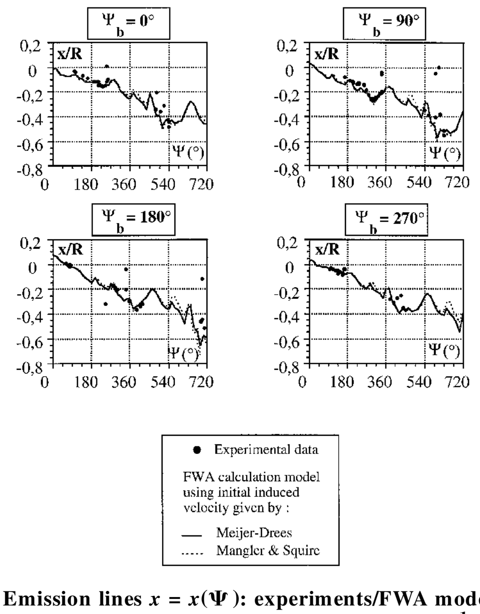

Fig. 9 Emission lines $x = x(\Psi)$: experiments/FWA model. $b = 2$, $\alpha_s = -12$ deg, $\mu = 0.2$, $\theta = 10$ deg, and $V_\infty = 21.4$ ms^{-1}.

As an example of the wake distortion predicted by the present free wake analysis (FWA) model, Fig. 9 provides a comparison between calculations and experiments concerning the wake geometry relative to the rectangular blades, at $\alpha_s = -12$ deg and $\mu = 0.20$. As previously mentioned, the calculation includes a free-wake analysis that is based on the experimental vortex core and intensity evolutions, and on the initial wake geometry description deduced from test data. It can be noticed that the mean-induced descent velocity of the tip vortex has been initialized using either the Meyer-Drees[15] model or the Mangler and Squire[17] model at the first calculation step of the model. From such an initial mean-induced velocity, the instantaneous descent velocity given by the $x/R = x/R(\Psi)$ evolution in Fig. 9 is then calculated using the present FWA model. The results presented in Fig. 9 clearly demonstrate the good efficiency of the present FWA model to provide a realistic distorted tip vortex path along the vertical x/R coordinate.

From the detailed knowledge of the wake geometry distortion and of the associated velocity field near the blade, three different types of blade/vortex interaction process have been identified and classified. Figure 10a shows the first type of interaction where the axis of the vortex shed by the preceding blade is perpendicular to the blade span. The typical associated three-dimensional velocity profiles, corresponding to such a BVI occurrence of type I, exhibit a significant amplitude variation mainly on the (u, v) velocity components. The pertur-

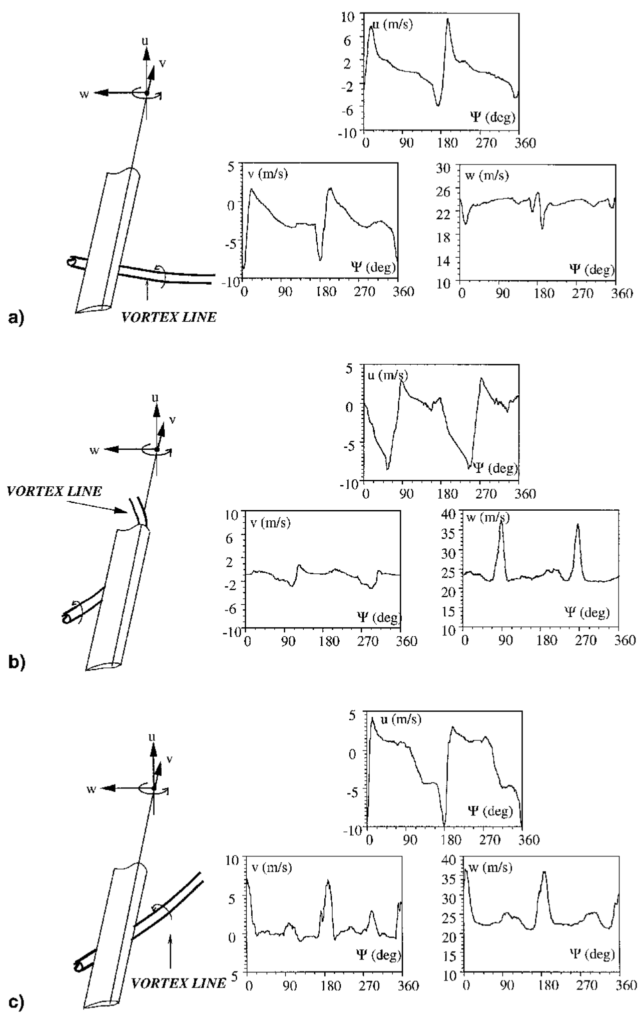

Fig. 10 Different types of BVI process. Types a) I, b) II, and c) III. $b = 2$, $\alpha_s = -12$ deg, $\mu = 0.2$, $\theta = 10$ deg, and $V_\infty = 21.4$ ms^{-1}.

bation generated in this case on the velocity field concerns only a reduced part of the blade span. The type II BVI process is characterized by a vortical emission where the axis of the vortex is nearly parallel to the blade span (see Fig. 10b). When compared to BVI of type I, the perturbation induced on the flowfield by the type II BVI process affects a larger zone of the blade span. In this case, the perturbation induces a significant amplitude variation in the (u, w) velocity components. The third type of BVI process in Fig. 10c corresponds to an intermediate position of the vortex axis orientation when compared to BVI types I and II. From such different types of BVI occurrence, the associated results concerning the vortex intensity and orientation with respect to the blade surface also appear to constitute valuable data for improvement and validation of aeroacoustic numerical models.

Conclusions

The present work has concerned an experimental and numerical investigation of rotor aerodynamics operating in forward flight.

The experiments were conducted by means of overall and local measurements and have been focused on determining the three-dimensional velocity field around the blade and in its wake and also on the wake geometry distortion generated in the forward-flight configuration. An effort to evaluate and improve the prediction efficiency of a rotor aerodynamic calculation method has been done by including an FWA option. This option has been based on a realistic time-dependent descent velocity of the tip vortex modeled in core radius and intensity along its path. The present FWA model has shown good predictions in modeling the associated wake geometry distortion as well as local aerodynamic parameters, including the spanwise circulation distribution at a given blade azimuth and the local three-dimensional velocity field.

Acknowledgment

The authors wish to thank the support provided by the Direction des Recherches Etudes et Techniques, under Grant 93/087.

References

[1]Biggers, J. C., and Orloff, K. L., "Laser Velocimeter Measurement of the Helicopter Rotor Induced Flow Field," *Proceedings of the 30th Annual National Forum of the American Helicopter Society* (Washington, DC), American Helicopter Society, Alexandria, VA, 1974, pp. 2–10.

[2]Nsi Mba, M., Meylan, C., Maresca, C., and Favier, D., "Radial Distribution Circulation of a Rotor in Hover Measured by Laser Velocimeter," *Proceedings of 10th European Rotorcraft* (The Hague, The Netherlands), 1984, pp. 1–14.

[3]Hoad, D. R., "Helicopter Local Blade Circulation Calculations for a Model Rotor in Forward Flight Using Laser Velocimeter Measurements," *Proceedings of the 47th Annual Forum of the American Helicopter Society* (Phoenix, AZ), American Helicopter Society, Alexandria, VA, 1991.

[4]Lorber, P. F., Stauter, R. C., Haas, R. J., and Anderson, T. J., "Techniques for Comprehensive Measurement of Model Helicopter Rotor Aerodynamics," *Proceedings of the 50th Annual Forum of the American Helicopter Society* (Washington, DC), American Helicopter Society, Alexandria, VA, 1994.

[5]Seelhorst, U., Beesten, B. M. J., and Butefish, K. A., "Flow Field Investigation of a Rotating Helicopter Rotor Blade by Three-Component Laser Doppler-Velocimeter," *AGARD-FDP on Aerodynamics and Acoustics of Rotorcraft, 75th Fluid Dynamics Panel Meeting*, AGARD, 1994, pp. 23.1–23.12 (Paper 23).

[6]Landgrebe, A. J., and Cheney, M. C., "Rotor Wake Key to Performance Prediction," *Proceedings of the AGARD-FDP on Aerodynamics of Rotary Wings* (Marseille, France), CP-111, AGARD, 1972, pp. 1.5–1.18.

[7]Egolf, T. A., and Landgrebe, A. J., "Helicopter Rotor Wake Geometry and Its Influence in Forward Flight. Volume I—Generalized Wake Geometry and Wake Effects on Rotor Airloads and Performance," NASA CR 3726, June 1983.

[8]Egolf, T. A., and Landgrebe, A. J., "Helicopter Rotor Wake Geometry and Its Influence in Forward Flight. Volume II—Wake Geometry Charts," NASA CR 3727, June 1983.

[9]Berton, E., Favier, D., and Maresca, C., "A New Method of Laser Velocimetry for Airloads Determination on Hovering Rotor Around Helicopter Rotor Blades," *Proceedings of 19th Aeronautical Sciences Congress* (Anaheim, CA), 1994, pp. 213–216.

[10]Ramos, J., Nsi Mba, M., Berton, E., Favier, D., and Silva, M., "A Laser Velocimetric Investigation of the Airloads and Performance of a Model Helicopter Rotor in Hover," *Proceedings of the American Helicopter Society Aeromechanics Specialists Conference* (San Francisco, CA), American Helicopter Society, Alexandria, VA, 1993, pp. 150–175.

[11]Toulmay, F., "Modeling of Rotor Aerodynamics (METAR)—Formulation and Application to Rotor SA 349-Blades G.V.," Aérospatiale, Rapport H/BE/R37176, 1986.

[12]Michea, B., "Study of Helicopter Rotor Wakes in Forward Flight; Effects on Rotor Performances," Thèse de Doctorat, Univ. de Paris VI, France, 1992.

[13]Favier, D., Maresca, C., Nsi Mba, M., and Berenger, T., "Experimental and Numerical Study of Helicopter Rotor Blade Aerodynamics in Forward Flight," Rapport à la Direction des Recherches Etudes et Techniques of the French Dept. of Defense, 92/061, April 1994.

[14]Berenger, T., "Experimental and Numerical Study of the Helicopter Vortical Wake in Forward Flight," Thèse de Doctorat, Univ. d'Aix-Marseille II, France, Dec. 1994.

[15]Meyer-Drees, J., "A Theory of Airflow Through Rotors and Its Applications to Some Helicopter Problem," *Journal of the Helicopter Association of Great Britain*, Vol. 3, No. 3, 1949, pp. 25–39.

[16]Rand, O., and Rosen, A., "An Unsteady Prescribed Wake Model for a Helicopter Rotor in Forward Flight," *Journal of the American Helicopter Society*, Vol. 30, No. 4, 1985, pp. 11–21

[17]Mangler, H. B., and Squire, R. W., "The Induced Velocity Field of a Rotor," NASA CR-2642, May 1950.